A&A 598, A65 (2017)
DOI: 10.1051/0004-6361/201629657

Astronomy & Astrophysics

Comparing the ρ and χ class spectra of the microquasar GRS 1915+105 observed with *Beppo*SAX

T. Mineo[1], M. Del Santo[1], E. Massaro[2,⋆], F. Massa[3,⋆], and A. D'Aì[1]

[1] INAF, Istituto di Astrofisica Spaziale e Fisica Cosmica di Palermo, via U. La Malfa 153, 90146 Palermo, Italy
e-mail: mineo@ifc.inaf.it
[2] INAF, Istituto di Astrofisica e Planetologia Spaziali, via del Fosso del Cavaliere 100, 00113 Roma, Italy
[3] INFN, Sezione Roma 1, Piazzale A. Moro 2, 00185 Roma, Italy

Received 6 September 2016 / Accepted 17 November 2016

ABSTRACT

Context. *Beppo*SAX observed GRS 1915+105 during two variability classes at the same 2–10 keV flux level. The ρ class is characterized by quasi-periodic flares recurring on a time-scale of 1 to 2 min, namely *heartbeat*, while the χ class is characterized by no strong temporal variability.
Aims. The aim of this work is to coherently analyze the source spectrum in these two classes and to gain insight into the source conditions that inset the *heartbeats*.
Methods. A single χ spectrum was accumulated, while ρ data were split in runs where five phase-resolved spectra were selected. In addition to the multicolor disc black body, the fitting model includes a hybrid Comptonization plus a Compton reflection component.
Results. Our results show that the emission in the ρ class is dominated by the multi-temperature disk, while in the χ class the Comptonised component is dominant. The disk temperature varies between a maximum of 1.95 ± 0.11 keV reached at the peak and a minimum of $0.95^{+0.08}_{-0.20}$ keV in the χ class. In both classes we detect a significant contribution from a non-thermal electron population to the total Comptonized emission. A broadened iron emission line is detected in the χ spectrum. We interpret the line shape as being due to reflection from an accretion disk extremely close to the black-hole ($R_{\rm in} = 4.1^{+1.5}_{-0.9}$ gravitational radii), with an equivalent width of 200 ± 20 eV. Concomitantly, upper limits of ∼150 eV can be derived from the ρ spectra.
Conclusions. In the framework of coupled disc-corona models, these results point out that the source emission is strongly affected by the fractions of accretion energy distributed between the disk, the corona, and possibly the wind, with no indication on the conditions that inset the *heartbeats*.

Key words. X-rays: binaries – X-rays: individuals: GRS 1915+105

1. Introduction

Since its discovery in 1992 (Castro-Tirado et al. 1992), GRS 1915+105 has become one of the best known and studied Galactic black-hole binaries (BHB). The system is a low-mass X-ray binary with a KIII companion star (Greiner et al. 2001) in a 34-day orbit. The latest value of the distance is $8.6^{+2.0}_{-1.6}$ kpc measured with the parallax method by Reid et al. (2014). These authors used data at 22.235 GHz collected with the Very Long Baseline Array (VLBA) at the National Radio Astronomy Observatory (NRAO). The newer value allowed for a revised estimation of the black-hole (BH) mass ($12.4^{+2.0}_{-1.8}\,M_{\odot}$) and of the system inclination ($60° \pm 5°$). There is evidence that the BH may be highly rotating with spin parameter a close to 1 (McClintock et al. 2006; Miller et al. 2013).

The X-ray emission of GRS 1915+105 is characterized by short and long-term variability patterns that give rise to an impressive phenomenology of light curves, involving peculiar spectral and timing features. A classification according to spectral hardness and timing features results in three main states (so-called A, B, and C states) and approximately 14 specific classes (Belloni et al. 2000; Klein-Wolt et al. 2002; Hannikainen et al. 2005).

The X-ray spectral behavior reflects the complex pattern of states with the presence of several components whose relative intensities and parameters vary with luminosity and temporal state (Done et al. 2004). The main contributions are due to thermal emission from the accretion disk and to Comptonization emission from a hot corona, whose electron distribution can be hybrid, having both thermal and non-thermal components (Zdziarski et al. 2005; Mineo et al. 2012). Depending on the mass accretion rate $\dot{M}$, the softer X-ray spectral component is described either with a standard α-disk model (Fender & Belloni 2004), or with the slim model (Vierdayanti et al. 2010). In addition, several other time-dependent spectral features have been observed in the X-ray band: fluorescence iron emission lines, originating from disk reflection (Martocchia et al. 2006; Ueda et al. 2010), and resonant absorption lines from highly ionized elements (Lee et al. 2002; Ueda et al. 2009; Neilsen & Lee 2009) indicating the presence of a radiatively supported disk wind.

In this paper, we focus on two specific variability classes: the ρ class, characterized by nearly regular bursting activity on minute time-scale, namely *heartbeats*, and the χ class characterized by a minimal level of temporal variability.

A detailed phase-resolved spectral analysis of the ρ class has been reported by Mineo et al. (2012) and by Neilsen et al. (2011, 2012) using *Beppo*SAX and RXTE data, respectively. The main

⋆ Retired.

contribution to the total luminosity in this class comes from the accretion disk (70%) whose temperature increases from ∼1 keV at the burst minimum up to ∼2 keV at the peak. The ρ burst series is characterized by a cycling behavior in a space of observable parameters such as the photon count-rate vs. the hardness ratio or the mean photon energy (see Massa et al. 2013). A physical model for describing this pattern was developed by Janiuk & Czerny (2005), while Massaro et al. (2014) used a non-linear system of two ordinary differential equations, adapted from the well-known Fitzhugh-Nagumo model, to reproduce the light and energy curves.

Broadband spectra in the χ class at a luminosity of 0.1–0.3 $L_{\rm Edd}$ have been studied by Zdziarski et al. (2005) with RXTE and CGRO/OSSE data and by Ueda et al. (2010) with a *Suzaku* observation at higher luminosity. In both works, the hybrid Comptonization model was used on the hard X-ray spectra and the disk contribution to the total flux was found to be lower than in the ρ class. However, Rodriguez et al. (2008b,a) and Fuchs et al. (2003) report on INTEGRAL and RXTE data collected in χ class where the disk parameters are not constrained and no non-thermal Comptonization component is required.

Here we present the analysis of a *Beppo*SAX observation of the source performed in 1999, when GRS 1915+105 was in the ρ class and we compare the spectral parameters with those obtained from a previous observation performed in 1996, when the source was in the χ class at a similar 2–10 keV flux level. The aim of this work is to obtain information on the disk luminosity and temperature in different physical conditions and to verify how the transition between them can be reproduced by means of mathematical models.

2. Observation and data reduction

We analyzed data from two *Beppo*SAX observations remaining to be unpublished: the first (ObsId 2025800800) was performed on November 15th, 1996, (see Table 1), and the second one (ObsId 2089900100) on April 13th, 1999, (see Table 2). The analysis is based on data obtained with the Medium Energy Concentrator Spectrometer (MECS), operating in the 1.3–10 keV energy band (Boella et al. 1997), and the Phoswich Detector System (PDS) operating in the 15–300 keV energy band (Frontera et al. 1997). Data from the Low Energy Concentrator Spectrometer (LECS) (0.1–10 keV; Parmar et al. 1997) are not considered, their exposures being significantly lower than those with MECS-PDS, that is, 100 s for the χ class and 15 ks distributed over all orbits for the ρ class. Data retrieved from *Beppo*SAX archive at the ASI Science Data Center (ASDC) were reduced and selected following the standard procedure and using the SAXDAS v. 2.3.3 package.

The MECS events for the timing and spectral analysis were selected within a circle of 8′ radius that contains approximately 95% of the point source signal. The relative background has been evaluated following the procedure suggested in the handbook for the spectral analysis[1]. We extracted the background at the edge of the field of view in the 1996 GRS 1915+105 observation and compared it with the one estimated from high Galactic latitude "blank" fields selecting a region with the same size and detector position. The ratio between the two rates is ∼30, and, even assuming that this ratio does not include contribution from the source, we obtain a flux (0.7 ct/s) that is negligible compared with the GRS 1915+105 one (see Table 1). The observation 2025800800 was performed before the switching-off of MECS1 in May 1997. Data are therefore relative to three units unlike the observation 2089900100 where only MECS2 and MECS3 are present.

Table 1. Log of the 1996 observation: ObsId 2025800800.

Orbit	T start (s)	Exposure (s)	Rate (ct/s) MECS*	PDS*
1	0	500	273.5 ± 11	31.1 ± 2
2	2910	2080	276.1 ± 10	33.2 ± 3
3	8688	2473	267.6 ± 10	33.4 ± 3
4	14 458	2919	299.1 ± 11	35.2 ± 4
5	20 119	2912	267.8 ± 12	33.8 ± 4

Notes. The columns list the sequential number of the orbits, the time in seconds from the starting time (1996 November 15 20:30:12 UTC), the exposure time and the rate detected in three MECS units. (*) Errors are computed in light curves with 10 s integration time bins with the rms with respect to the average along the orbit, to be compared with the average Poisson error that is 5 ct/s for the MECS and 2 ct/s for the PDS.

PDS was operated in the standard rocking mode and the background was obtained from contemporary measurements.

Spectral analysis was performed with XSPEC v.12.7.0 using the response matrices available from the *Beppo*SAX archive[2]. The MECS-PDS intercalibration factor was left free to vary in the range 0.83–0.89 as expected for point sources with a high count-rate[3].

Data collected in 1999, when the source was in ρ class, have been split into runs and named following the criteria adopted by Massaro et al. (2010). Each series corresponds to a continuous observing period and is tagged with the letter *P* followed by the orbit sequential number (Table 2). The analysis is performed over runs that have an exposure higher than 1000 s in order to have sufficient statistics.

3. Temporal analysis

3.1. 1996 observation: χ class

We estimated the variability of the X-ray emission, computing the mean rate averaged over each orbit in the 1.6–10 keV (MECS) and 15–100 keV (PDS) bands (see Table 1 and Fig. 1) in light curves with 10 s integration time bin and found that it is ∼10% at maximum. Moreover, the rms, with respect to the mean within each orbit (quoted in Table 1 in parenthesis), are at a level of 2σ of the Poissonian fluctuations. Hardness ratios using 1.6–5.0 keV, 5.0–10.0 keV and 13–100 keV energy bands have been computed and no significant variation was detected.

Belloni et al. (2000) identified two classes with low-amplitude variation, namely ϕ and χ, distinguished on the basis of the value of the RXTE hardness ratios between counts in the ranges 5–13 keV and 2–5 keV (HR_1) and that in the 13–60 keV and 2–5 keV bands (HR_2). In particular, for observations in χ mode, HR_2 is always >0.1 and the HR_1 – HR_2 color–color diagram shows points that are diagonally elongated (see Figs. 2c,d in Belloni et al. 2000). Points relative to the ϕ class instead occupy a different region of the diagram being characterized by the values of HR_1 ≈ 1 and HR_2 ≈ 0.05 (see Figs. 2a, b in Belloni et al. 2000).

We used the same criterion to identify the class computing a conversion factor between *Beppo*SAX and RXTE hardness

[1] ftp://ftp.asdc.asi.it/sax/doc/software_docs/saxabc_v1.2.ps.gz

[2] http://www.asdc.asi.it/bepposax

[3] http://www.asdc.asi.it/bepposax/software/cookbook

Table 2. Log of the 1999 observation: ObsId 2089900100.

Series	T start (s)	Exposure (s)	Rate (ct/s) MECS	PDS
P1	0.0	2417.6	232.4	55.5
P2b	6215.3	2011.5	226.0	53.1
P3b	12 443.3	1600.1	211.0	48.8
P4a	16 654.2	1135.2	207.2	45.3
P4b	18 666.3	1019.9	214.9	49.5
P5a	22 484.0	1436.5	205.8	45.0
P6a	28 254.5	1785.1	209.0	44.8
P7	34 019.3	2162.4	209.9	45.3
P8	39 785.6	2496.2	203.7	44.6
P9	51 343.3	3104.6	206.3	45.2
P10	56 973.5	3255.2	198.3	43.2
P11	62 746.5	3246.8	197.6	43.8
P12a	68 722.5	1530.2	198.7	44.9
P12b	69 926.5	1914.0	198.7	44.9
P13	74 448.7	3127.2	196.6	43.7
P14a	80 451.5	1150.2	200.3	44.0
P15	86 617.5	2467.3	204.2	47.1
P16b	92 842.4	1587.3	207.3	49.3

Notes. The columns list the names of the runs, the time in seconds since April 13th, 1999, 2:11:34 UT, the exposure time and the count rates in the two MECS units and in the PDS.

ratios. In particular, we defined HR_2 in the same bands as Belloni et al. (2000) while taking into account the different MECS energy band. HR_1 is computed in the energy intervals 5–10 keV and 2–5 KeV. The factors to convert the *Beppo*SAX hardness ratios into the RXTE ones are mainly determined by the difference in the effective area between the instruments. We then evaluated these factors simulating in XSPEC (command FAKEIT) the RXTE spectrum corresponding to the best fit model in the *Beppo*SAX data (see Sect. 4.2). Using the simulated RXTE rates in the selected bands, we found that *Beppo*SAX HR_1 and HR_2 are 0.46 and 0.69 times the RXTE values, respectively.

The color–color diagram for *Beppo*SAX data gave points all above HR_2 > 0.15, that, applying the conversion factors, corresponds to 0.22 for RXTE, with a slightly diagonal elongation. These results indicate that the source was in the χ mode.

3.2. 1999 observation: ρ class

A detailed temporal analysis of this observation has been presented in Mineo et al. (2016) and therefore we summarize here the main results of the analysis. We evaluated the mean recurrence time of the bursts $T_{\rm rec}$ and the hard X delay (*HXD*), defined as the delay between the evolution of the count rate and the average energy in each burst, with the methods presented in Massaro et al. (2010) and Massa et al. (2013) for another dataset collected in 2000 (Obs_2000). They confirmed the positive correlation between $T_{\rm rec}$ and *HXD* with the rate at the minimum of each burst *BL*. However, in the April 1999 observation the source brightness was within the range detected in Obs_2000 but with a time evolution that also includes a decreasing interval, the $T_{\rm rec}$ and *HXD* values are distributed in two parallel branches in their plot with respect to *BL*. Comparing these results with those of Obs_2000 (Massa et al. 2013), we find that the upper branch corresponds well with the Obs_2000 trend while the other branch is systematically lower.

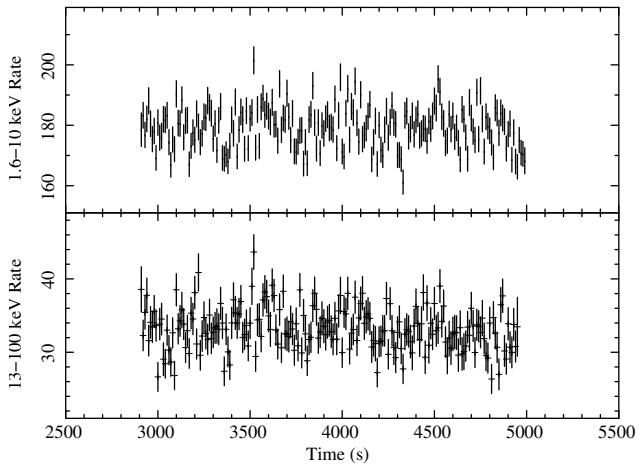

Fig. 1. Light curves collected in one orbit of the 1996 observation with 10 s integration time bins. The *top panel* shows the 1.6–10 keV rate observed with the two telescope units MECS2 and MECS3, while the PDS rates in the range 13–100 keV are presented in the *bottom panel*.

4. Spectral analysis

Broad-band spectra were fitted with the hybrid Comptonization model developed by Coppi (1999; EQPAIR in XSPEC), while in our previous work (Mineo et al. 2012) we used the COMPPS model developed by Poutanen & Svensson (1996). Both models assume that all photons produced in the disk are Comptonised by corona electrons. However they have a different approach to deriving the source emission: EQPAIR assumes that the input electron energy distribution is known, and derives the equilibrium temperature of the thermal plasma distribution while the final contribution of the non-thermal electrons is computed from the solutions of the energy exchange equations. In COMPPS, the electron state distribution is composed of a thermal distribution up to a given energy and a power law above it. From these it computes the Comptonized emission.

Two main reasons brought us to adopt EQPAIR: i) COMPPS cannot fit the 1996 χ class spectrum ($\chi^2_\nu = 1.4$ for 253 d.o.f.); ii) in the ρ class the reflection fraction was very high ($\Omega > 1$) but, inconsistently, we could not detect a corresponding iron emission line: the 3σ upper limit on the equivalent width (EW) was ~50 eV.

In our fits with EQPAIR, we assumed a spherical corona with the size of the scattering region fixed at 10^7 cm and composed of electrons (XSPEC param $pairinj = 0$) with Maxwellian distribution at low energy and non-thermal distribution at high energy. This electron plasma is illuminated by a geometrically thin disk in a pseudo-Newtonian potential (Paczyński & Wiita 1980) and a temperature distribution parametrized by its maximum ($T_{\rm max}$). The disk has an inclination of 60° and is composed of gas with an average temperature of 10^6 K. The inner radius was fixed at six gravitational radii ($r_{\rm g} = GM/c^2$), even if the GRS 1915+105 harbors a rapidly rotating black hole (McClintock et al. 2006; Miller et al. 2013), because this is the lower limit accepted by the model.

We assumed that the non-thermal distribution is a power law between the Lorenz factors $\gamma_{\rm min} = 1.3$ and $\gamma_{\rm max} = 1000$ as adopted by Gierliński et al. (1999) for Cygnus X-1. Because of the lack of high-energy data, we fixed the spectral index of the non-thermal distribution $\Gamma_{\rm inj}$ at 2.5 as expected from the shock acceleration model (i.e., Del Santo et al. 2016).

Table 3. Best fit spectral parameters for the χ and ρ classes.

Paramater	χ class	ρ class*				
		$SLT-1$	$SLT-2$	$P-1$	$P-2$	FDT
$N_{\rm H}$ (10^{22} cm^{-2})	$6.57^{+0.03}_{-0.02}$	6.70 ± 0.16	7.24 ± 0.13	7.97 ± 0.16	7.57 ± 0.19	6.53 ± 0.19
$kT_{\rm max}$ (keV)	$0.94^{+0.08}_{-0.20}$	1.26 ± 0.02	1.21 ± 0.02	1.41 ± 0.05	1.95 ± 0.11	1.57 ± 0.06
$\ell_{\rm h}/\ell_{\rm s}$	$0.60^{+0.02}_{-0.01}$	0.29 ± 0.02	0.24 ± 0.02	0.14 ± 0.02	0.11 ± 0.03	0.31 ± 0.03
$\ell_{\rm nth}/\ell_{\rm th}$	$0.22^{+0.01}_{-0.02}$	0.05 ± 0.08	0.14 ± 0.08	0.30 ± 0.14	0.34 ± 0.11	0.36 ± 0.14
τ	$1.10^{+0.14}_{-0.09}$	0.18 ± 0.04	0.13 ± 0.02	0.08 ± 0.03	0.31 ± 0.13	0.26 ± 0.05
ξ	<0.68	0.0	0.0	0.0	0.0	0.0
Ω	$0.77^{+0.17}_{-0.08}$	0.0	0.0	0.0	0.0	0.0
E (keV)	$6.46^{+0.03}_{-0.02}$	–	–	–	–	–
$R_{\rm in}$	$4.1^{+1.5}_{-0.9}$	–	–	–	–	–
$\beta_{\rm line}$	$3.0^{+0.09}_{-0.33}$	–	–	–	–	–
θ (deg)	86^{+2}_{-3}	–	–	–	–	–
EW (eV)	200 ± 20 eV	–	–	–	–	–
$F_{\rm total}{}^{\dagger}$	5.45	3.7 ± 0.3	5.0 ± 0.4	7.6 ± 0.3	7.0 ± 0.6	3.82 ± 0.27
$F_{\rm disk}^{\dagger}$	1.88	2.69 ± 0.18	3.84 ± 0.22	6.42 ± 0.46	5.91 ± 0.69	2.69 ± 0.20
$F_{\rm disk}$ (% fraction of total)	34	72.7 ± 4.9	76.9 ± 4.4	84.5 ± 6.1	84.5 ± 9.9	70.4 ± 5.3
$F_{\rm cor}$ (% fraction of total)	59	27.3 ± 4.9	23.0 ± 4.4	15.5 ± 6.1	15.5 ± 9.9	29.5 ± 5.3

Notes. (*) We assume the standard deviation of the distribution of the best fit values in each group of spectra as error. (†) 0.01–200 keV unabsorbed flux in unit of 10^{-8} erg cm^{-2} s^{-1}.

The properties of the plasma depend on the undimensional compactness parameter defined as:

$$\ell = \frac{\sigma_{\rm T}}{m_{\rm e}c^3}\frac{L}{R}, \quad (1)$$

where L is a power (luminosity) of the source supplied by different components (i.e., *soft* from the disk or *hard* from the more energetic electrons), R is the radius of the source, $\sigma_{\rm T}$ is the Thomson cross-section, $m_{\rm e}$ is the electron mass and c is the speed of light.

The up-scattered spectrum mainly depends on the ratio between the power supplied to the accelerated electrons and the power of the soft photons coming from the disk. This is handled by the model with the ratio between the two relative compactness parameters defined in Gierliński et al. (1999) $\ell_{\rm h}/\ell_{\rm s}$ where $\ell_{\rm h}$ is relative to the electrons and includes both thermal and non-thermal contribution ($\ell_{\rm h} = \ell_{\rm th} + \ell_{\rm nth}$), and $\ell_{\rm s}$ is relative to the disk.

It is customary to fix the soft compactness $\ell_{\rm s}$ (named $\ell_{\rm bb}$ in XSPEC) because data do not allow its constraint. Several values of $\ell_{\rm s}$ have been used to fit GRS 1915+105 spectra in χ class: $\ell_{\rm s} = 10$ adopted by Del Santo et al. (2013) and Gierliński et al. (1999) in other black holes, $\ell_{\rm s} = 100$ adopted by Zdziarski et al. (2005) for the analysis of a RXTE observation of GRS 1915+105, and $\ell_{\rm s} = 1000$ used by Ueda et al. (2010) on *Suzaku* data. We fitted a sample of spectra in the two classes with these values and found that our data are compatible with 10 and 100, while 1000 can be definitively ruled out on the basis of the reduced χ^2. We adopted the value of 10 on all fits.

In the latest EQPAIR code (v1.04), the Compton reflection (IREFLCT) is computed with the method of Magdziarz & Zdziarski (1995) considering ionized material and taking into account the relativistic blurring. The model normalization Ω is the solid angle of the cold reflecting matter to the illuminating source expressed in units of 2π.

The iron line is fitted with a model suitable for the rapidly rotating Kerr black hole (LAOR in XSPEC; Laor 1991) that assumes a line emissivity with a power law dependence from the disk radius $\Phi \propto r^{\beta_{\rm line}}$. We used the XSPEC model TBABS with cross-sections from Verner et al. (1996) and element abundance from Wilms et al. (2000) for the low-energy absorption.

4.1. 1996 observation: χ class

Since there is no evident spectral variation in the χ class, a single spectrum was accumulated. The whole time-averaged spectrum fitted with EQPAIR provided an acceptable fit with a reduced χ^2 of 1.17 (252 d.o.f.); the values of the free parameters are shown in Table 3 with errors reported at 90% confidence level, the energy spectrum plus the model, and the residuals in units of σ are plotted in the top left panel of Fig. 3.

In this class, we found that the power supplied to the electron plasma is 60% of the Comptonized soft photon power and that the non-thermal electrons contribute 22% of the total hard power. When fixing $\ell_{\rm nth}/\ell_{\rm h}$ to zero, we obtained an unacceptable reduced χ^2, which means that our high-energy data require a significant fraction of non-thermal Comptonization as also previously reported (Zdziarski et al. 2005; Ueda et al. 2010).

The disk contributes 30% of the total luminosity and has a $kT_{\rm max}$ temperature of $0.94^{+0.08}_{-0.20}$ keV comparable to that found by Ueda et al. (2010), while it is a factor of two lower than the temperatures found by Zdziarski et al. (2005).

The Compton reflection component is required by our data ($\Omega = 0.77^{+0.17}_{-0.08}$) with a value higher than that reported in

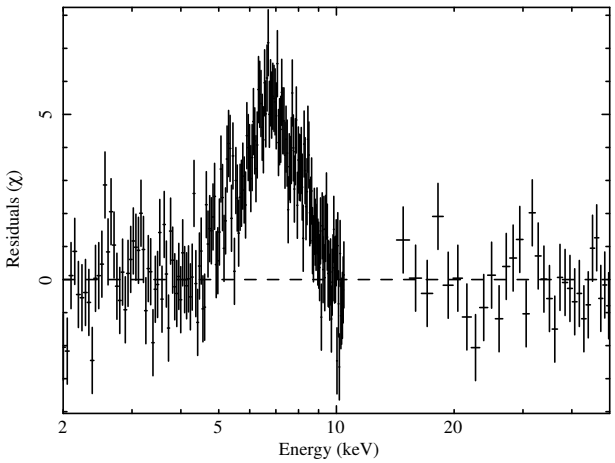

Fig. 2. Residuals in units of χ with respect to the best fit model where the iron line flux is set to zero.

Ueda et al. (2010), while it is in agreement with Zdziarski et al. (2005).

A cold iron line with an EW of 200 ± 20 eV is found at $6.46^{+0.03}_{-0.02}$ keV in agreement with the low value of the upper limit on the ionization parameter ($\xi < 0.68$). The value of the index of the emissivity dependence with the radius ($\beta_{\rm line} = 3.0^{+0.09}_{-0.33}$) as well as the line profile (see Fig. 2) shows that the line is strongly dominated by emission from the inner part of the disk (Laor 1991). The best fit of the inner radius ($4.1^{+1.5}_{-0.9}$ $r_{\rm g}$) is moreover consistent with the value assumed in EQPAIR. The inclination of the disk estimated from the line profile (86^{+2}_{-3} deg) is higher than the inclination measured with the rotational parameter of the system (Reid et al. 2014). However, a tilt of the disk inner region with respect to the orbit's plane is expected in the Kerr black hole disks where the gas tends to align its angular momentum to the BH one (Bardeen & Petterson 1975). Slightly lower inclination values have been found by Miller et al. (2013) using a relativistically blurred disk reflection model on *NuStar* data.

We further investigated whether or not the non-thermal component is requested by our data. Following Rodriguez et al. (2008b,a) and Fuchs et al. (2003), we used a multi-color black body plus a Gaussian and a power law. Despite this model being able to fit MECS data well, it produces large residuals when extended to the broad band spectra (reduced $\chi^2 = 253(191)$).

4.2. 1999 observation: ρ class

The ρ class spectral analysis was performed dividing each burst into five phase-selected segments (see Fig. 4). The first two segments SLT–1 and SLT–2 are the two halves of the slow leading trail (SLT), which goes from the minimum level up to half height of the pulse (P). The latter was also divided into two equal segments P–1 and P–2. The fifth segment is the fast decaying tail (FDT) of the burst. A spectrum for each of these five segments was accumulated in all runs (see Mineo et al. 2012, for details).

All 90 accumulated spectra have been fitted with EQPAIR. We do not detect a reflection component nor any emission iron line in the ρ class spectra. As an example, energy spectra and residuals of the SLT–1, P–1, and FTD intervals for the P12b run are shown in the top right and in the bottom panels of Fig. 3, respectively.

The best fit parameters averaged over the 18 runs for each of the five spectra are shown in Table 3 and plotted in Figs. 5 and 6. Errors represent the rms with respect to the mean in each interval, they are also consistent with the statistical errors at the 90% confidence level, as we verified on a sample of spectra. Figure 7 shows the percentage of the disk and corona fluxes of the total luminosity.

We found the maximum inner disk temperatures to be in good agreement with those reported by Mineo et al. (2012) and by Neilsen et al. (2011, 2012). The disk temperature increases from ∼1.2 keV in the SLTs up to ∼2 keV at the peak, during which the disk flux almost doubles.

The absorbing column density varies in correlation with the phase, showing higher values (maximum increase ∼20%) closer to the burst peak (see Table 3). To investigate the possibility that this change is due to a false spectral modeling of the emission in the low-energy band, we fitted a sample of spectra with DISKPBB. In this model, the dependence of the disk temperature on radius is given by a power law with a slope that is one of the free parameters of the fit. In addition, we used an empirical model SIMPL to mimic the thermal Comptonization. However, this first approximation is only valid up to 30 keV. Leaving the $N_{\rm H}$ column as a free parameter, a maximum variation of ∼10% was obtained with an anti-correlation with the source luminosity; while fixing the column to the average value gave acceptable fit for all spectra.

5. Discussion

Systematic studies of the spectral behavior of this source in different variability classes were performed by several authors (Done et al. 2004; Muno et al. 1999; Belloni et al. 2000). Here we have focused on the comparison between two classes. We can schematically summarize the main spectral changes in the two states as follows:

- *Low energy absorption*: the value detected in the χ class is statistically compatible with those relative to the SLT–1 and FDT intervals. The increase up to 20% along the burst is correlated with the luminosity as already found in Mineo et al. (2012). The detailed analysis performed in this paper and in Obs_2000 with several complex, low-energy absorptions and different disk models shows that the moderate-energy resolution and the effective area of the MECS below 2 keV do not allow for disentanglement of the correlation between the $N_{\rm H}$ and the luminosity.
- *Disk*: the temperature and the luminosity of the disk component in the χ class spectrum are significantly lower than the values in all the segments of ρ bursts. The contribution to the total luminosity is also significantly different in the two classes: it decreases from the 70–85% of the ρ class to the 34% of the χ class.
- *Corona*: the corona dominates the χ class emission, while its contribution is strongly reduced in the spectra of the ρ class. The physical status is also different in the two classes: the gas is moderately ionized in the χ class with an optical depth of ∼2 and becomes completely neutral and optically thin ($\tau = 0.1$) in the ρ class when the flux of the underling disk increases up to a factor of three. Electrons receive a larger fraction of power in the χ class (72%) with respect to the ρ class where they get a maximum of 30%, while the fraction of non-thermal electrons is equivalent in the two classes (∼30%).
- *Compton reflection and iron line*: significant Compton reflection is detected in the χ class only. The observed strong relativistic line is produced close to the last stable orbit for a rapidly rotating BH. Detection of iron line in GRS 1915+105 spectrum has been reported in several

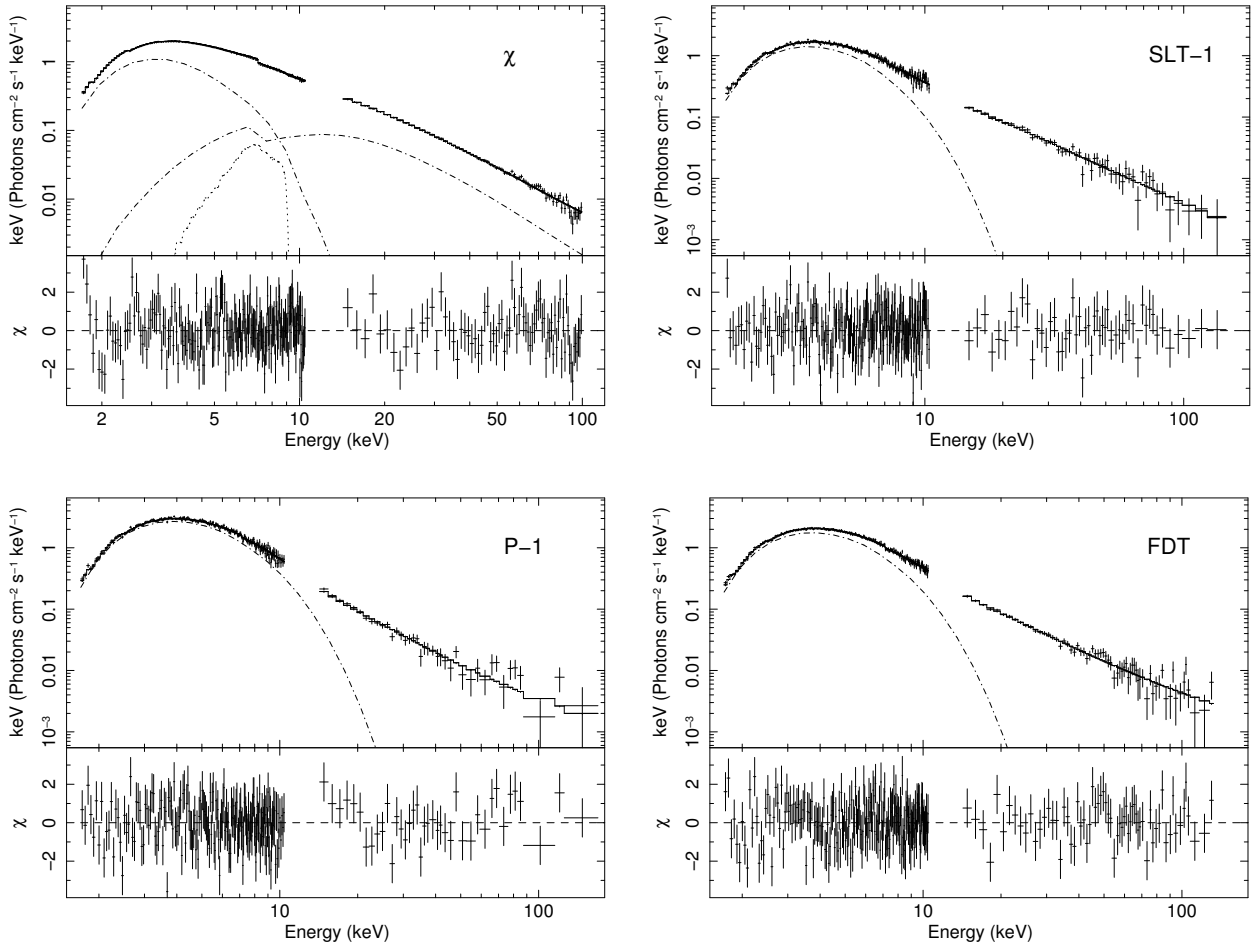

Fig. 3. Energy spectra, best fit model, and residuals for the χ class (*top left panel*), and for $SLT-1$ (*top right panel*), the $P-1$ (*bottom left panel*) and FDT (*bottom right panel*) of the P12b run. The single black body and reflection components are also plotted (dash-dot lines).

observations (Zdziarski et al. 2005; Martocchia et al. 2006; Titarchuk & Seifina 2009; Ueda et al. 2010; Miller et al. 2013). However, evidence for a relativistic line has only been reported by Martocchia et al. (2002) with *Beppo*SAX observations in time intervals when the source showed low variability.

During the ρ class, the iron line disappeared coherently with the absence of the reflection bump. The upper limit at the 2σ level on the line EW (150 eV) and on the reflection component ($\Omega < 2$) is higher than the values estimated in the χ class. This may be due to the strong contribution of the disk emission, which covers the reflection component: we cannot completely exclude its presence.

The comparison of the spectral results of the two classes suggests that an equivalent accretion rate of the system is redistributed between the corona and the disk in two different fractions. This fraction f cannot be directly computed from the EQPAIR paramater ℓ_h/ℓ_s because of the reprocessing of the hard X-rays in the disk. A formula that takes this phenomenon into account is given by Kubota & Done (2016):

$$f = g\,\frac{2 - C_r + C_r\,e^{-\tau}}{1 + e^{-\tau} - g(1 - C_r\,e^{-\tau})}, \quad (2)$$

with

$$g = \frac{\ell_h}{(\ell_h + \ell_s)},$$

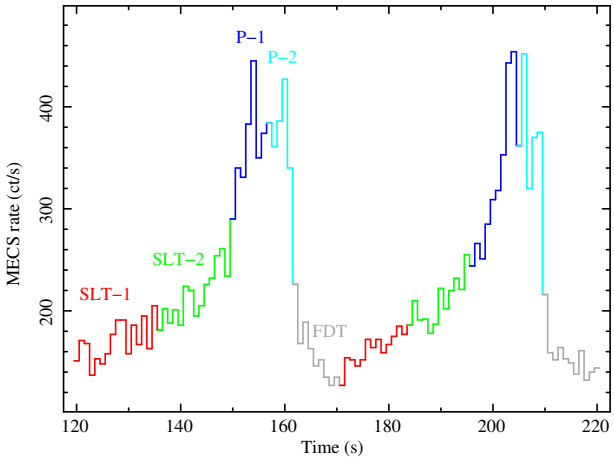

Fig. 4. Segment of the light curve corresponding to the run P2b. The color indicates the five segments used for the spectral analysis.

where C_r is the fraction of corona photons irradiating the disk that are reflected without reprocessing in the disk ($C_r = 1$ means no reprocessing). Our results indicate that the fraction of power injected into the corona for the χ class spectrum is 0.4 and 0.8 for $C_r = 1$ and $C_r = 0$, respectively, and it has a value of approximately 0.2, independently from C_r in all the ρ class spectra.

A different evaluation of the $\dot{M}$ in the disk can be obtained by applying the formula $A6$ in Gierliński et al. (1999) that links

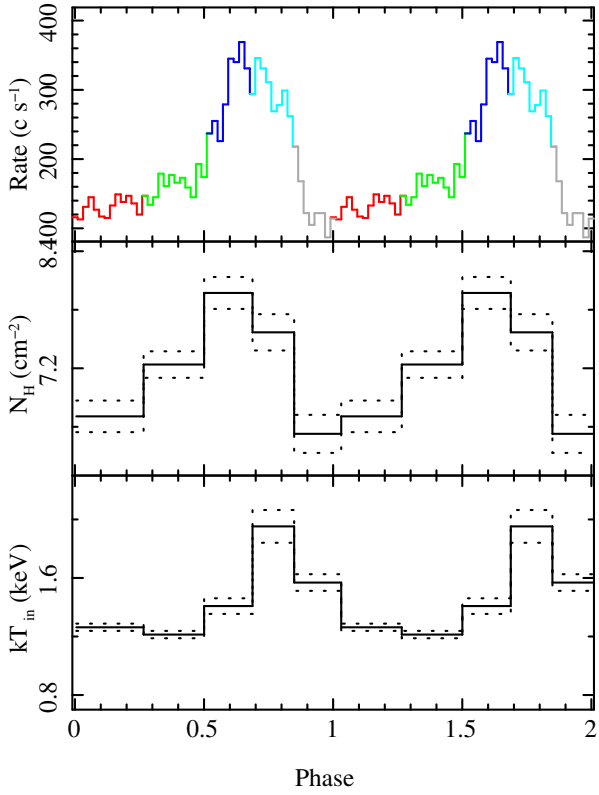

Fig. 5. Continuous black lines indicate the average of the best fit absorption column (*middle panel*) and inner disk temperature (*bottom panel*) in the five intervals; dashed lines show the interval relative to the rms. For comparison, in the *top panel*, the light curve of one burst is plotted.

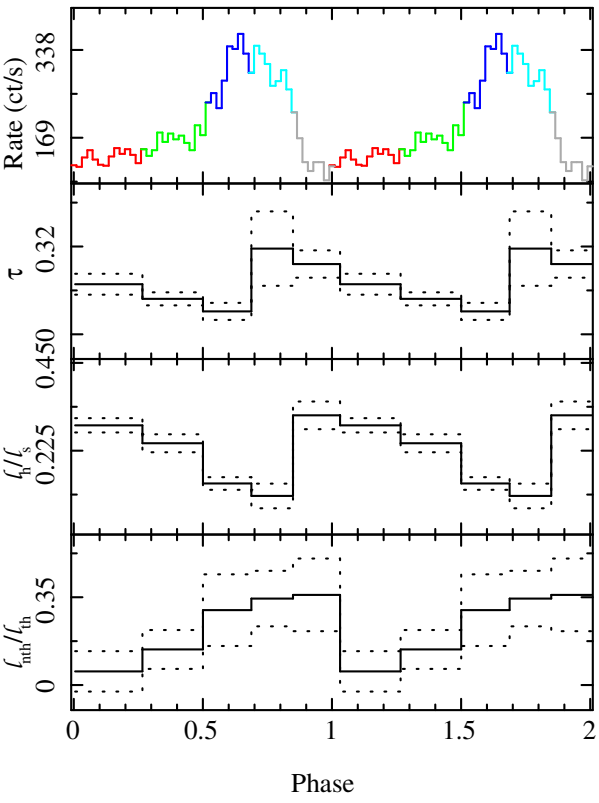

Fig. 6. Continuous black lines indicate the average of the best fit τ (*second panel*), ℓ_h/ℓ_s (*third panel*) and ℓ_{nt}/ℓ_h (*bottom panel*) in the five intervals; dashed lines show the interval relative to the rms. For comparison, in the *top panel* the light curve of one burst is plotted.

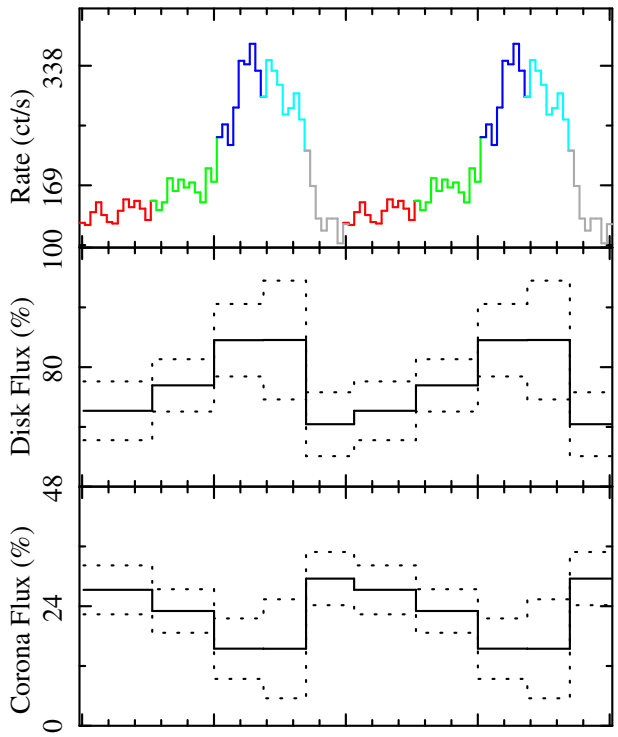

Fig. 7. Contribution in percentage of the total flux provided by the disk (*middle panel*) and by the corona (*lower panel*). The dashed lines show the interval relative to the rms. For comparison, in the *top panel*, the light curve of one burst is plotted.

it to the fourth power of the maximum temperature, if the disk reaches the last stable orbit. Considering that we detect a relativistic line in the χ class spectrum and high disk temperatures in the ρ class we can assume that this condition is valid. To overtake the variation of the temperature along the burst, probably due to a complex viscosity in act during the *heartbeats*, we computed the average temperature (1.47 keV). The fourth power of the ratio of the two temperatures foresees almost a factor of ten increase of $\dot{M}$ between the two classes, which is approximately twice the highest estimate computed with Eq. (2). However, the disk temperature in a system with a significant fraction of energy injected in the corona is different, typically with a lower temperature, when compared to a state with a faint corona. This is caused by strong coupling between the two components (Kubota & Done 2016). The two results, therefore, bring us to the same conclusion that the corona is energetically dominant in the χ class.

In conclusion, the fraction of energy injected into the system is differently distributed in the disk and in the corona in the two classes. The disk is well modeled by DISKPN relative to a stable state also in the ρ class when the source is in bursting mode. The state of the disk is strongly affected by the oscillation during the ρ class and by the coupling with the corona in the χ class and no simple theoretical relation can be used to model the luminosity/temperature evolution. This physical description of the source should also take into account the link between radio emission and X-ray states (Rushton et al. 2010; Rodriguez et al. 2008a; Klein-Wolt et al. 2002; Muno et al. 2001), because the coronal emission could be related to the existence of compact jet. We inspected the radio flux observed by Ryle at the Mullard Radio Astronomy Observatory at 15 GHz and indeed find that the radio flux is ~25 mJy during *Beppo*SAX χ observation, and ~3 mJy when the source is in the ρ class (Pooley 2006).

Finally, we highlight the possibility that a limit-cycle behavior responsible for the oscillation in the innermost region of the disk can be justified in the framework of the slim disk model (Honma et al. 1991; Szuszkiewicz & Miller 1998), while its presence in the standard disk model can be obtained if the role of a corona is also taken into account (Janiuk et al. 2000, 2002; Janiuk & Czerny 2005). The importance of the role of the wind in stabilising the oscillations has recently been investigated by Janiuk et al. (2016) who found that, assuming a constant fraction of the source mass accretion rate involved in the wind, the code is able to reproduce the *hearthbeat* oscillation of the IGR 17091-3624. Moreover, to suppress the oscillations it is sufficient to increase the wind strength.

6. Summary and conclusion

We analyzed two unpublished *Beppo*SAX observations of GRS 1915+105 at a similar X-ray luminosity level but in two different variability classes, χ and ρ. The averaged χ spectrum and the phase resolved ρ spectra were modeled with EQPAIR. We found that the χ class did not show any spectral variation along the observing period, at variance with the ρ class where different spectral parameters have been observed to change along the burst. The disk is always well modeled by a standard stable disk with a maximum value of temperature at the burst peak (~2 keV) and a minimum in the χ spectrum (~0.9 keV). In the ρ class, the emission was dominated by the multi-temperature disk, while in the χ class the Comptonised component is dominant. In both classes a statistically significant contribution from the non-thermal Comptonized component is required with equivalent fractions of the non-thermal population. A strong relativistic line is observed in the χ spectrum ($EW \sim 110$ eV), while only upper limits are obtained in the phase resolved spectra of the ρ classes.

These results point out that the source emission is strongly affected by the fractions of accretion energy distributed between the disk, the corona, and, possibly, the wind, with no indication on the conditions that inset the *heartbeats*.

Acknowledgements. The authors thank Julien Malzac for his valuable and helpful comments and suggestions on the paper. The authors also thank M. Capalbi, for help in retrieving and reducing *Beppo*SAX archive data. This work has been partially supported by research funds of the Sapienza Università di Roma. M.D.S. acknowledges financial contribution from the agreement ASI-INAF I/037/12/0.

References

Bardeen, J. M., & Petterson, J. A. 1975, ApJ, 195, L65
Belloni, T., Klein-Wolt, M., Méndez, M., van der Klis, M., & van Paradijs, J. 2000, A&A, 355, 271
Boella, G., Chiappetti, L., Conti, G., et al. 1997, A&AS, 122, 327
Castro-Tirado, A. J., Brandt, S., & Lund, N. 1992, IAU Circ., 5590, #2, ed. D. W. E. Green
Coppi, P. S. 1999, in High Energy Processes in Accreting Black Holes, eds. J. Poutanen, & R. Svensson, ASP Conf. Ser., 161, 375
Del Santo, M., Malzac, J., Belmont, R., Bouchet, L., & De Cesare, G. 2013, MNRAS, 430, 209
Del Santo, M., Belloni, T. M., Tomsick, J. A., et al. 2016, MNRAS, 456, 3585
Done, C., Wardziński, G., & Gierliński, M. 2004, MNRAS, 349, 393
Fender, R., & Belloni, T. 2004, ARA&A, 42, 317
Frontera, F., Costa, E., dal Fiume, D., et al. 1997, A&AS, 122, 357
Fuchs, Y., Rodriguez, J., Mirabel, I. F., et al. 2003, A&A, 409, L35
Gierliński, M., Zdziarski, A. A., Poutanen, J., et al. 1999, MNRAS, 309, 496
Greiner, J., Cuby, J. G., McCaughrean, M. J., Castro-Tirado, A. J., & Mennickent, R. E. 2001, A&A, 373, L37
Hannikainen, D. C., Rodriguez, J., Vilhu, O., et al. 2005, A&A, 435, 995
Honma, F., Kato, S., Matsumoto, R., & Abramowicz, M. A. 1991, PASJ, 43, 261
Janiuk, A., & Czerny, B. 2005, MNRAS, 356, 205
Janiuk, A., Czerny, B., & Siemiginowska, A. 2000, ApJ, 542, L33
Janiuk, A., Czerny, B., & Siemiginowska, A. 2002, ApJ, 576, 908
Janiuk, A., Grzedzielski, M., Sukova, P., et al. 2016, ArXiv e-prints [arXiv:1604.02888]
Klein-Wolt, M., Fender, R. P., Pooley, G. G., et al. 2002, MNRAS, 331, 745
Kubota, A., & Done, C. 2016, MNRAS, 458, 4238
Laor, A. 1991, ApJ, 376, 90
Lee, J. C., Reynolds, C. S., Remillard, R., et al. 2002, ApJ, 567, 1102
Magdziarz, P., & Zdziarski, A. A. 1995, MNRAS, 273, 837
Martocchia, A., Matt, G., Karas, V., Belloni, T., & Feroci, M. 2002, A&A, 387, 215
Martocchia, A., Matt, G., Belloni, T., et al. 2006, A&A, 448, 677
Massa, F., Massaro, E., Mineo, T., et al. 2013, A&A, 556, A84
Massaro, E., Ventura, G., Massa, F., et al. 2010, A&A, 513, A21
Massaro, E., Ardito, A., Ricciardi, P., et al. 2014, Ap&SS, 352, 699
McClintock, J. E., Shafee, R., Narayan, R., et al. 2006, ApJ, 652, 518
Miller, J. M., Parker, M. L., Fuerst, F., et al. 2013, ApJ, 775, L45
Mineo, T., Massaro, E., D'Ai, A., et al. 2012, A&A, 537, A18
Mineo, T., Massa, F., Massaro, E., & D'Aì, A. 2016, A&A, 586, A56
Muno, M. P., Morgan, E. H., & Remillard, R. A. 1999, ApJ, 527, 321
Muno, M., Remillard, R., Morgan, E., et al. 2001, Ap&SS, 276, 227
Neilsen, J., & Lee, J. C. 2009, Nature, 458, 481
Neilsen, J., Remillard, R. A., & Lee, J. C. 2011, ApJ, 737, 69
Neilsen, J., Remillard, R. A., & Lee, J. C. 2012, ApJ, 750, 71
Paczyńsky, B., & Wiita, P. J. 1980, A&A, 88, 23
Parmar, A. N., Kahabka, P., Hartmann, H. W., et al. 1997, A&A, 323, L33
Pooley, G. G. 2006, in VI Microquasar Workshop: Microquasars and Beyond, 19.1
Poutanen, J., & Svensson, R. 1996, ApJ, 470, 249
Reid, M. J., McClintock, J. E., Steiner, J. F., et al. 2014, ApJ, 796, 2
Rodriguez, J., Hannikainen, D. C., Shaw, S. E., et al. 2008a, ApJ, 675, 1436
Rodriguez, J., Shaw, S. E., Hannikainen, D. C., et al. 2008b, ApJ, 675, 1449
Rushton, A., Spencer, R. E., Pooley, G., & Trushkin, S. 2010, MNRAS, 401, 2611
Szuszkiewicz, E., & Miller, J. C. 1998, MNRAS, 298, 888
Titarchuk, L., & Seifina, E. 2009, ApJ, 706, 1463
Ueda, Y., Yamaoka, K., & Remillard, R. 2009, ApJ, 695, 888
Ueda, Y., Honda, K., Takahashi, H., et al. 2010, ApJ, 713, 257
Verner, D. A., Ferland, G. J., Korista, K. T., & Yakovlev, D. G. 1996, ApJ, 465, 487
Vierdayanti, K., Mineshige, S., & Ueda, Y. 2010, PASJ, 62, 239
Wilms, J., Allen, A., & McCray, R. 2000, ApJ, 542, 914
Zdziarski, A. A., Gierliński, M., Rao, A. R., Vadawale, S. V., & Mikołajewska, J. 2005, MNRAS, 360, 825